arXiv:1608.06055v1 [cond-mat.str-el] 22 Aug 2016

Charge and orbital order due to cooperative Jahn-Teller effect in manganite chains

Ravindra Pankaj and Sudhakar Yarlagadda
CMP Division, Saha Institute of Nuclear Physics, Kolkata, India
(Dated: August 23, 2016)

We derive an effective Hamiltonian that takes into account the quantum nature of phonons and models cooperative Jahn-Teller effect in the adiabatic regime and at strong electron-phonon coupling in one dimension. Our approach involves mapping a strong-coupling problem to a weak-coupling one by using a duality transformation. Subsequently, a sixth-order perturbation theory is employed in the polaronic frame of reference where the small parameter is inversely (directly) proportional to the coupling (adiabaticity). We study charge and orbital order in ferromagnetic manganite chains and address the pronounced electron-hole asymmetry in the observed phase diagram. In particular, at strong coupling, we offer an explanation for the observed density dependence of the wavevector of charge modulation, i.e., wavevector is proportional to (independent of) electron density on the electron-doped (hole-doped) side of the phase diagram of manganites. We also provide a picture for the charge and orbital order at special fillings $\frac{1}{2}$, $\frac{1}{3}$, $\frac{1}{4}$, and $\frac{1}{5}$; while focusing on the ordering controversy at fillings $\frac{1}{3}$ and $\frac{1}{4}$, we find that Wigner-crystal arrangement is preferred over bi-stripe order.

PACS numbers: 71.38.-k, 71.45.Lr, 75.47.Lx, 71.38.Ht

I. INTRODUCTION

Various transition-metal oxides such as manganites [1–14], cuprates [15], nickelates [16], cobaltates [17], etc. display clear evidence for stripe-like magnetic and charge orders. In doped Mott insulators such as cuprates and nickelates, it has been argued that stripes are generated by the competition between the clustering tendency of the doped holes (in regions of suppressed antiferromagnetism) and the long-range Coulomb interactions [18]. On the other hand, properties in manganites arise as a compromise between the tendency of the carriers to delocalize owing to the kinetic energy and their propensity to localize due to a strong cooperative Jahn-Teller (CJT) effect and the antiferromagnetic (AFM) interaction between the Mn core spins. *Here, we show that the CJT effect produces long-distance repulsion thereby enabling stripe formation.*

Perovskite manganites $R_{1-x}A_xMnO_3$ (R = La, Pr, Sm, etc., A = Sr, Ca, etc.) exhibit a zoo of exotic phases involving a variety of spin, charge, and orbital textures/stripes. The stripe phases involve A-, C-, or CE-type antiferromagnets [19]; they manifest charge orders that have doping dependent wavevectors above $x = 0.5$ and doping independent wavevectors below $x = 0.5$ [7, 20]; and reveal C-type, ferro-type, Wigner-crystal/bi-stripe orbital orders [21].

Among the charge-ordered manganites, low-bandwidth manganites such as $Pr_{1-x}Ca_xMnO_3$ (PCMO) display charge-ordering for fairly large range of doping, namely, $0.3 \leq x \leq 0.75$ [1, 19, 22]; whereas intermediate-bandwidth manganites such as $La_{1-x}Ca_xMnO_3$ (LCMO) exhibit charge-ordering for $0.5 \leq x \leq 0.8$[23, 24]. At $x = 0.5$, checker-board charge ordering is manifested in both PCMO and LCMO with ordering wavevector $k = 0.5a^*$, where a^* is reciprocal lattice vector [19, 21]. On the other hand, at $x = 2/3$ and $x = 3/4$ there is a controversy whether a bi-stripe order or a Wigner-crystal order is realized by the system [9, 23, 25, 26]. Furthermore, for $0.8 \lesssim x \lesssim 0.85$ in LCMO, orbital order (without charge order) involving d_{z^2} orbitals along ferromagnetic chains in a C-type antiferromagnet has been reported [23]. Additionally, at $0.3 < x < 0.5$ in $Pr_{1-x}Ca_xMnO_3$, it has been claimed that CE-type checker-board order (corresponding to $x = 0.5$) is retained with excess electrons occupying the Jahn-Teller compatible d_{z^2} orbitals at the empty sites of the checker board [19]. *Here, we present a scenario for Wigner-crystal states at $x = 2/3$ and $x = 3/4$ and a C-AFM state for $x \gtrsim 0.8$. Furthermore, we also offer an explanation for the Jahn-Teller compatible states realized for $x < 0.5$ in narrow-band compounds such as PCMO.*

Evidence of sizeable local Jahn-Teller distortions indicating strong electron-phonon coupling has been provided in manganites by direct techniques such as extended x-ray absorption fine structure [27] and pulsed neutron diffraction [28]. For a long time, charge ordering in the overdoped regime ($x > 0.5$) was considered arising from ordered arrangement of Mn^{3+} and Mn^{4+} ions, i.e., stripes of localized charges [29]; for arbitrary dopings, charge-ordering was thought to be a fine mixture of two adjacent commensurate configurations according to the lever rule [25]. This scenario (purported to result from strong-coupling) has been questioned based on experiments which show that the charge modulation continues to be uniform when passing from commensurate to incommensurate filling [6, 7]. *In this article, we show that even strong coupling at an incommensurate filling produces a finite peak in the structure factor with wavevector that is linearly dependent on filling ν $(= 1 - x)$ and rules out charge stacking faults.*

As regards theoretical efforts, double exchange, superexchange, and Coulombic repulsion have been utilized to study manganites. Jahn-Teller effect (without

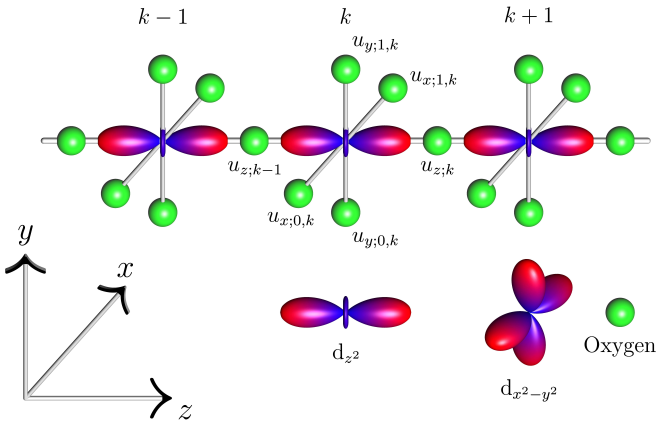

FIG. 1. (Color online) Depiction of one-dimensional cooperative Jahn-Teller interaction in a chain involving d_{z^2} and $d_{x^2-y^2}$ orbitals and oxygen ions. For simplicity, only d_{z^2} orbitals and oxygen ions are displayed in the chain and their locations are indicated.

cooperativity) was used additionally to explain colossal magnetoresistance in the conducting regime of the manganites [30, 31]. On the other hand, a number of experiments suggest Jahn-Teller effect, with cooperativity, to be crucial in stabilizing charge ordering in LCMO (at $x \geq 0.5$) and PCMO (at $x > 0.3$) [1, 26, 32–34]. However, an effective Hamiltonian that models CJT effect is yet to be developed; consequently, there does not exist a unified picture that explains the rich phase diagram of manganites. *In the present work, employing perturbation theory up to sixth order, we obtain an effective Hamiltonian that models CJT effect (by taking into account quantum phonons) in the intermediate- and narrow-band manganites in one dimension.* In these lower tolerance materials, the small parameter is sufficiently small since it is directly proportional to the adiabaticity which is not too large and inversely proportional to the electron-phonon coupling which is large due to large polaronic distortion [35]. Our study is relevant to the insulating regime $x \geq 0.5$ ($x \geq 0.3$) of intermediate- (narrow)-band manganites where either zigzag or straight ferromagnetic chains are antiferromagnetically coupled. *In our one-dimensional model, we demonstrate particle-hole asymmetry by obtaining the observed CDW-wavevector dependence on density* [7, 20].

II. EFFECTIVE POLARONIC HAMILTONIAN

We consider a one-dimensional Jahn-Teller chain with cooperative electron-phonon interaction along the z-direction and non-cooperative electron-phonon interaction (of the Holstein-type [36, 37]) along the x- and y-directions as shown in Fig. 1. We consider spinless fermions so as to model the physics of ferromagnetic chains. We write the Hamiltonian for cooperative-Jahn-Teller chain as follows (see Appendix A for details):

$$\begin{aligned} H^{CJT} =& -t\sum_k (d^\dagger_{1,k+1}d_{1,k} + \text{H.c.}) \\ & - g\omega_0 \sum_k \Big[(a^\dagger_k + a_k)(n_{1,k} - n_{1,k+1}) \\ & \quad + \frac{1}{2}(b^\dagger_k + b_k)(n_{1,k} + 3n_{2,k}) \\ & \quad - \frac{\sqrt{3}}{2}(c^\dagger_k + c_k)(d^\dagger_{1,k}d_{2,k} + \text{H.c.})\Big] \\ & + \omega_0 \sum_k (a^\dagger_k a_k + b^\dagger_k b_k + c^\dagger_k c_k), \end{aligned} \tag{1}$$

where $n_{1,k} \equiv d^\dagger_{1,k}d_{1,k}$ and $n_{2,k} \equiv d^\dagger_{2,k}d_{2,k}$ with $d^\dagger_{1,k}$ ($d^\dagger_{2,k}$) being the creation operator for d_{z^2} ($d_{x^2-y^2}$) orbital; phonon creation and annihilation operators are defined as follows:

$$\begin{aligned} \frac{a^\dagger_k + a_k}{\sqrt{2M\omega_0}} &= u_{z;k}, \\ \frac{b^\dagger_k + b_k}{\sqrt{2\frac{M}{4}\omega_0}} &= (u_{x;1,k} - u_{x;0,k}) + (u_{y;1,k} - u_{y;0,k}), \\ \frac{c^\dagger_k + c_k}{\sqrt{2\frac{M}{4}\omega_0}} &= (u_{x;1,k} - u_{x;0,k}) - (u_{y;1,k} - u_{y;0,k}), \end{aligned}$$

where u_x, u_y, and u_z are, respectively, displacements of the oxygens along x-, y-, and z-axes (See Fig. 1).

We will now modify the Lang-Firsov transformation [38] and apply it to the above Hamiltonian so that we can perform perturbation in the polaronic (Lang-Firsov transformed) frame of reference. The transformed Hamiltonian is given by $\tilde{H}^{CJT} = \exp(S)H^{CJT}\exp(-S)$ where

$$\begin{aligned} S =& -g\sum_k [(a^\dagger_k - a_k)(n_{1,k} - n_{1,k+1}) \\ & + \frac{1}{2}(b^\dagger_k - b_k)(n_{1,k} + 3n_{2,k})]. \end{aligned} \tag{2}$$

Here, in our modified Lang-Firsov transformation, it should be noted that we have included only the density terms and ignored the orbital-flip terms ($d^\dagger_{1,k}d_{2,k}$ and its Hermitian conjugate) appearing in the interaction part of the above equation (1). This choice is dictated by mathematical expediency to arrive at an analytic expression. Then, the Lang-Firsov transformed Hamiltonian is given by $\tilde{H}^{CJT} = H_{\text{ph}} + H_{\text{s}} + H_1$ where

$$H_{\text{ph}} = \omega_0 \sum_k (a^\dagger_k a_k + b^\dagger_k b_k + c^\dagger_k c_k), \tag{3}$$

and

$$\begin{aligned} H_{\text{s}} =& -te^{-(E_p+V_p)/\omega_0}\sum_k (d^\dagger_{1,k+1}d_{1,k} + \text{H.c.}) \\ & -E_p\sum_k (n_{1,k} + n_{2,k}) + 2V_p\sum_k n_{1,k}n_{1,k+1}, \end{aligned} \tag{4}$$

with $E_p = \frac{9}{4}g^2\omega_0$ being the polaronic energy and $2V_p = 2g^2\omega_0$ being the repulsion between nearest-neighbor (NN) d_1-electrons due to cooperative interaction. In Eq. (4), it is important to note that there is no interaction between NN d_2-electron and d_1-electron or between two NN d_2-electrons. The remaining term is the perturbation:

$$H_1 \approx -te^{-\frac{E_p+V_p}{\omega_0}} \sum_k [d^\dagger_{1,k+1} d_{1,k} \{\mathcal{T}^{k\dagger}_+ \mathcal{T}^k_- - 1\} + \text{H.c.}], \quad (5)$$

where $\mathcal{T}^k_\pm \equiv \exp[\pm g(2a_k - a_{k-1} - a_{k+1}) \pm \frac{g}{2}(b_k - b_{k+1})]$. The details of the exact transformation along with the perturbation theory are given in Appendix B. For realistic values of adiabaticity and electron-phonon coupling in manganites, we need to retain dominant terms up to sixth order in perturbation as will be explained below. Now, while performing perturbation theory, the NN repulsion between two d_1-electrons must be carefully accounted for; hence, in the dominant-interaction processes considered in Fig. 2, we differentiate between situations where the mobile d_1-electron does not interact interact with another d_1-electron [see Figs. 2(c), 2(e), 2(g)] and those where the mobile d_1-electron does interact with another d_1 electron [see Figs. 2(d), 2(f), 2(h)].

The second-order term reads as follows:

$$\begin{aligned} H^{II}_{\text{eff}} &= \sum_m \frac{\langle 0|_{ph} H_1 |m\rangle_{ph} \langle m|_{ph} H_1 |0\rangle_{ph}}{E^{ph}_0 - E^{ph}_m} \\ &= -\frac{t^2}{E_p + 2V_p} e^{-\frac{E_p}{\omega_0}} \sum_k P_{k+1} \left[d^\dagger_{1,k+2} d_{1,k} + \text{H.c.} \right] \\ &\quad - \frac{t^2}{2E_p + 2V_p} \sum_k P_{k+1} \big[n_{1,k}(1 - n_{1,k+2}) \\ &\qquad + n_{1,k+2}(1 - n_{1,k}) \big] \\ &\quad - \frac{t^2}{2E_p + 4V_p} \sum_k P_{k+1} \big[n_{1,k} n_{1,k+2} + n_{1,k+2} n_{1,k} \big], \quad (6) \end{aligned}$$

where $P_{k+1} \equiv (1 - n_{1,k+1})(1 - n_{2,k+1})$ projects out electrons at site $k+1$. In the above equation, on the right-hand side (RHS), the expression containing $d^\dagger_{1,k+2} d_{1,k}$ in the first term represents next-nearest-neighbor (NNN) hopping as displayed in Fig. 2(a) (see Appendix B and Ref. 39 for details). It should be noted that Fig. 2(b) does not contribute to the second-order term since NN repulsion is large. The expression containing $n_{1,k}(1 - n_{1,k+2})$ in the second term on the RHS corresponds to Fig. 2(c) and Figs. 3(a) and 3(b); here, NNN site is unoccupied by d_1-electron and the lattice distortion remains unchanged while the electron hops to the neighboring site and returns back. The denominator $2E_p + 2V_p$ in the second term on the RHS is the difference of the energies of the intermediate state and the initial state; the origin of the denominator is explained as follows. The initial state shown in Fig. 3(a) has energy $-E_p$ whereas the intermediate state depicted in Fig. 3(b) has energy $E_p + 2V_p$; in the energy of the intermediate state, $+E_p$ arises due to the distortion without the electron whereas $2V_p$ contribution is from the repulsion between the electron and the oxygen ion displaced towards it. Next, the expression containing $n_{1,k} n_{1,k+2}$ in the the last term on the RHS is depicted in Fig. 2(d) and Figs. 3(c) and 3(d) with NNN site being occupied by d_1-electron; here, the energy of the intermediate state [Fig. 3(d)] is $2E_p + 4V_p$ above the ground state with $4V_p$ representing repulsion felt by the electron at site $k+1$ due to neighboring oxygens displaced towards it on both the sides. The last two terms on the RHS indicate repulsion between NNN electrons only if no electron is present between them. Here it should be noted that, while carrying out perturbation theory, we assumed $te^{-(E_p+V_p)/\omega_0} << \omega_0$ which is valid for manganites. Furthermore, the small parameter of our perturbation theory is $\sqrt{\frac{t^2}{(2E_p+2V_p)\omega_0}} = \sqrt{\frac{2}{13}}\frac{t}{g\omega_0}$; it is obtained from the following largest coefficients in $2l$-order processes which involve the electron hopping l times back and forth between NN sites while NNN site is not occupied by d_1-electron [for a similar analysis for a Holstein model, see Ref. 40]:

$$\left(\frac{t^2}{(2E_p + 2V_p)\omega_0} \right)^l \omega_0 \sum_k P_{k+1} \big[n_{1,k}(1 - n_{1,k+2}) + n_{1,k+2}(1 - n_{1,k}) \big].$$

Thus we have shown that *the polaronic (Lang-Firsov) transformation is actually a duality transformation that maps the original strong-coupling problem in Eq.* (1) [*with perturbation proportional to* $(g\omega_0)/t$] *to a weak-coupling problem* [*with small parameter proportional to* $t/(g\omega_0)$] [41].

The dominant contribution for the next-to-next-nearest neighbor (NNNN) interaction is given by fourth-order processes and expressed below (for clarity on the associated lattice distortions, see Fig. 8 in Appendix D):

$$\begin{aligned} H^{IV}_{\text{eff}} &= -\frac{t^4}{\big(2E_p + 2V_p\big)^2 \big(2E_p\big)} \\ &\quad \times \sum_k P_{k+1} P_{k+2} \left[n_{1,k} \Big(1 - \frac{V_p}{E_p + V_p} n_{1,k+3} \Big) \right. \\ &\qquad \left. + n_{1,k+3} \Big(1 - \frac{V_p}{E_p + V_p} n_{1,k} \Big) \right]. \quad (7) \end{aligned}$$

In the above equation, the expression containing $n_{1,k}\Big(1 - \frac{V_p}{E_p+V_p} n_{1,k+3}\Big)$ is obtained by considering the processes depicted in Figs. 2(e) and 2(f). We first note that, if an oxygen is displaced towards the new location of the mobile electron in any intermediate state, the energy of the intermediate state is enhanced further by $2V_p$ with respect to the ground state [see Figs. 8(b), 8(e), and 8(f)]. Regarding the virtual hopping to the site $k+1$ in Fig. 2(e) or in Fig. 2(f), the intermediate state has energy $2E_p + 2V_p$ above the ground state. Next, associated with virtual hopping to the site $k+2$ in Fig. 2(f) [Fig. 2(e)],

the intermediate state has energy $2E_p + 2V_p$ $[2E_p]$ above the ground state.

Lastly, the sixth-order processes leading to the dominant contribution for the next-to-next-to-next-nearest neighbor (NNNNN) repulsion are depicted in Figs. 2(g) and 2(h) and yield the following expression:

$$H_{\rm eff}^{VI} = -\frac{t^6}{\left(2E_p+2V_p\right)^2\left(2E_p\right)^3} \times \sum_k \prod_{i=1,2,3} P_{k+i}\Big[n_{1,k}\Big(1-\frac{V_p}{E_p+V_p}n_{1,k+4}\Big) + n_{1,k+4}\Big(1-\frac{V_p}{E_p+V_p}n_{1,k}\Big)\Big]. \quad (8)$$

Then, up to sixth order in perturbation, the effective Hamiltonian for the CJT chain is given by

$$H_{\rm eff}^{CJT} = H_{\rm s} + H_{\rm eff}^{II} + H_{\rm eff}^{IV} + H_{\rm eff}^{VI}. \quad (9)$$

Interestingly, in our effective Hamiltonian, presence of an in-between electron completely blocks the repulsion between the two surrounding electrons, i.e., screening is 100% in contrast to long-range Coulomb repulsion. Here, it should also be pointed out that odd order (such as third or higher order) in perturbation theory leads to hopping terms that are negligible compared to all the terms (including the NN and NNN hopping terms) in Eq. (9).

III. ANALYSIS OF CJT MODEL

Owing to the large on-site inter-orbital repulsion, there exists only three possibilities, i.e., site is unoccupied or occupied by either a d_1-electron or a d_2-electron. The size of the Hilbert space is 3^N where N is the total number of sites. However, for a fixed number N_1 of d_1-electrons and N_2 of d_2-electrons, it further reduces to ${}^{N}C_{N_p} \times {}^{N_p}C_{N_1}$ with $N_p = N_1 + N_2$ being the total number of particles. We diagonalize the effective Hamiltonian in Eq. (9) using modified Lanczos algorithm [42] for fixed values of N, N_p, and N_1 to obtain the minimum energy state of the system when electron-phonon coupling $g = 2.3$ and adiabaticity $\frac{t}{\omega_0} = 3.0$.

To identify the charge and orbital ordering, we study the correlations of the particles. The two-point correlation function for density fluctuations of $d_{a(b)}$-electrons with $a(b) = 1, 2$ is given by

$$W_{d_a d_b}(l) = \frac{4}{N}\sum_j \left[\langle n_{a,j} n_{b,j+l}\rangle - \langle n_{a,j}\rangle\langle n_{b,j+l}\rangle\right], \quad (10)$$

where $\langle n_{a,j}\rangle = \frac{N_a}{N}$. Then, the observable structure factor is expressed as the Fourier transform of $W_{d_a d_b}(l)$ as follows:

$$S_{d_a d_b}(k) = \sum_l e^{ikl} W_{d_a d_b}(l), \quad (11)$$

where the wavevector $k = \frac{2n'\pi}{N}$ with $n' = 1, 2, \ldots, N$ and lattice constant taken to be of unit length.

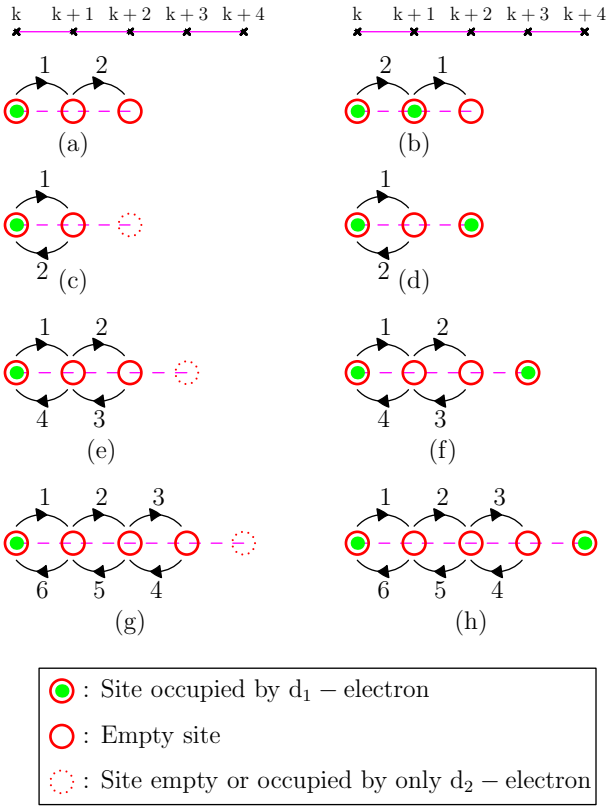

FIG. 2. (Color online) Schematic depiction of processes yielding dominant interaction terms in perturbation theory. In second-order perturbation, (a) a single particle hopping forward twice; (b) two particles sequentially hopping forward; (c) [(d)] a particle hopping to NN site and returning while NNN site is unoccupied [occupied] by d_1-electron. In fourth-order perturbation, (e) [(f)] a particle hopping to NNN site and coming back while NNNN site is unoccupied [occupied] by d_1-electron. In sixth-order perturbation, (g) [(h)] a particle hopping to NNNN site and coming back while NNNNN site is unoccupied [occupied] by d_1-electron. The numbered arrows indicate the order of hopping.

A. Up to half-filling case

We display lowest energies of the CJT system as a function of number of d_2-electrons in Fig. 4(a). We observe from this figure that, for the ground state up to half filling, electrons occupy only the d_{z^2} orbitals whereas $d_{x^2-y^2}$ orbitals remain unoccupied. Hence, up to half filling, i.e., $\nu = \frac{N_p}{N} \leq \frac{1}{2}$, we need to consider only one-orbital case for further study. Consequently, in the ground state, $N_p = N_1$ as $N_2 = 0$ and the Hilbert space reduces to ${}^{N}C_{N_1}$ for a fixed number of particles. Instead of using modified Lanczos algorithm, we do full exact diagonalization of the effective Hamiltonian in Eq. (9) so as to avoid problems due to degeneracy; we calculate correlation functions, structure factor, and excitation energies.

At strong coupling and in the adiabatic regime which are relevant to the manganites, we will analyze correlation function and structure factor for the ground

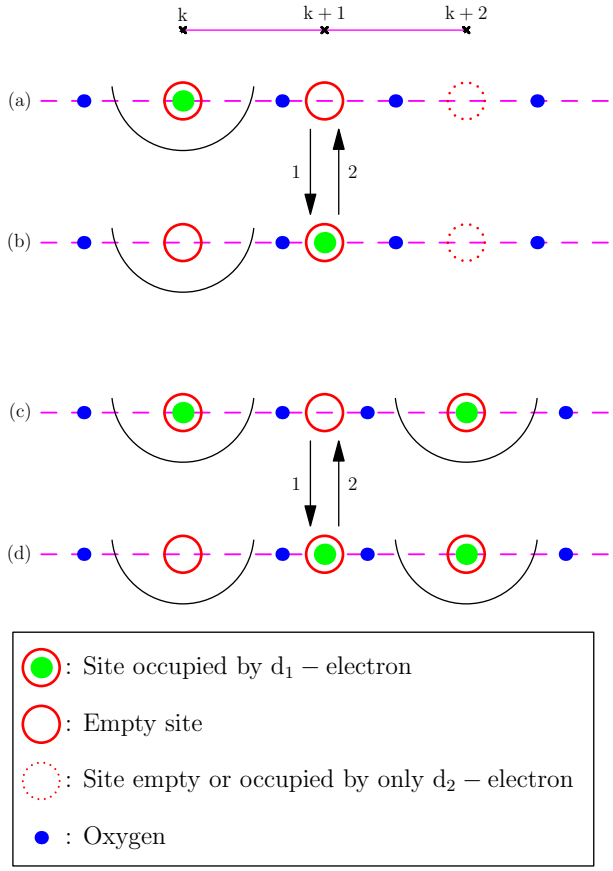

FIG. 3. (Color online) Display of initial/final and intermediate states with concomitant lattice distortions in a second order perturbation process with electron hopping to NN site and coming back. When NNN site is unoccupied by d_1-electron: (a) initial/final state and (b) intermediate state. When NNN site is occupied by d_1-electron: (c) initial/final state and (d) intermediate state. The order of hopping is specified by the numbered arrows.

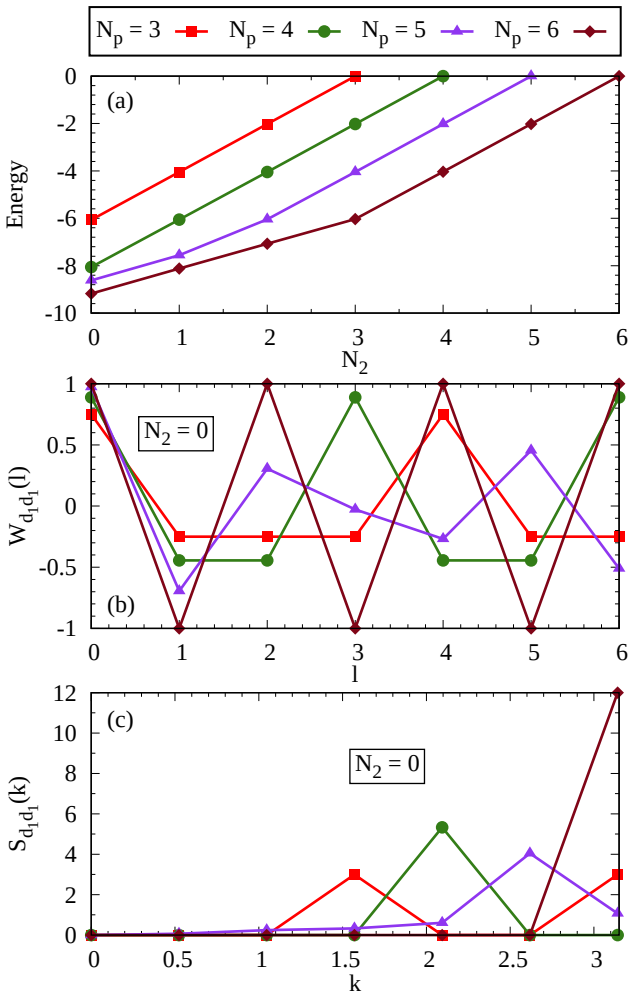

FIG. 4. (Color online) Plots of (a) lowest energy (in units of $\frac{t^2}{2E_p+2V_p}$) excluding the polaronic energy; (b) correlation function $W_{d_1d_1}(l)$; and (c) structure factor $S_{d_1d_1}(k)$ at filling $\nu \leq 1/2$ in a straight chain with periodic boundary condition. The chain has $N = 12$ sites and N_p electrons of which N_2 are d_2-electrons; electron-phonon coupling $g = 2.3$ while adiabaticity $\frac{t}{\omega_0} = 3.0$. At $\nu = 1/n$, $W_{d_1d_1}(l = m/\nu) = 4\nu(1-\nu)$ and $W_{d_1d_1}(l \neq m/\nu) = -4\nu^2$; and we get charge order with $S_{d_1d_1}(k) = 4N_p^2/N$ at the reported wavevector $k = 2\pi\nu$ [7, 20] and 0 otherwise.

state. We display the two-point correlation function in Fig. 4(b); we observe that the system at strong coupling and in the adiabatic regime has oscillatory correlation function with fixed amplitude for special fillings such as $\frac{1}{2}$, $\frac{1}{3}$, and $\frac{1}{4}$. At the above mentioned special fillings, from the excitation gaps in Table. I and Fig. 4(b), it is evident that the system has an insulating CDW state with ordering wavevector $2\pi\nu$ as depicted by structure factor peaks in Fig. 4(c). For special fillings, as will be explained below, $S_{d_1d_1}(k)$ peaks attain their maximum value for $k = 2\pi\nu$ and zero everywhere else when the particles are strongly localized at their respective periodic positions in the lattice.

Away from the above mentioned special fillings, system does not have long range order as reflected by the not so regular behavior of the correlation function in Fig. 4(b). Away from special fillings, system has short range correlations corresponding to the wavevector $2\pi\nu$ as shown by the peak in the structure factor in Fig. 4(c). In contrast to special fillings, structure factor for non-special fillings is not zero away from $k = 2\pi\nu$. As will be shown below, at $\nu \neq 1/n$ with n being an integer, the system is metallic in the absence of disorder; whereas, in the presence of even weak disorder, the system becomes insulating with a finite peak expected in the structure factor at $k = 2\pi\nu$.

At special fillings $\nu = 1/n$ with n being an integer, when system is in a charge ordered state with particles separated by distances m/ν, it is interesting to note that we can simplify Eqs.(10) and (11) in the following way. Since particles are absent at a distance $l \neq \frac{m}{\nu}$ where $m = 1, \ldots, N\nu$, $\langle n_{1,j} n_{1,j+l} \rangle = 0$. Therefore, Eq. (10)

reduces to

$$W_{d_1 d_1}\left(l \neq \frac{m}{\nu}\right) = -\frac{4N_p^2}{N^2} = -4\nu^2. \quad (12)$$

When particles are present at a distance $l = \frac{m}{\nu}$, $\sum_j \langle n_{1,j} n_{1,j+l}\rangle = N_p$. Hence, Eq. (10) simplifies to

$$W_{d_1 d_1}\left(l = \frac{m}{\nu}\right) = 4\nu(1-\nu). \quad (13)$$

Now, the contribution of the correlation term $\sum_j \langle n_{1,j} n_{1,j+l}\rangle$ to the structure factor is given by [see Eqs. (10) and (11)]

$$S^c_{d_1 d_1}(k) = \frac{4}{N}\sum_l e^{ikl}\sum_j \langle n_{1,j} n_{1,j+l}\rangle$$
$$= \frac{4}{N}\sum_{m=1}^{N\nu} e^{ik\frac{m}{\nu}} N\nu. \quad (14)$$

On the other hand, contribution of the mean-field term $\sum_j \langle n_{1,j}\rangle\langle n_{1,j+l}\rangle$ to the structure factor is

$$S^m_{d_1 d_1}(k) = \frac{4}{N}\sum_l e^{ikl}\sum_j \langle n_{1,j}\rangle\langle n_{1,j+l}\rangle$$
$$= 4N\nu^2\delta_{k,0}. \quad (15)$$

Next, from Eq. (14), we note that $S^c_{d_1 d_1}(k = 2\pi\nu p) = 4N\nu^2$ and $S^c_{d_1 d_1}(k \neq 2\pi\nu p) = 0$ for integer values of p with $0 \leq p < n$. Since $S_{d_1 d_1}(k) = S^c_{d_1 d_1}(k) - S^m_{d_1 d_1}(k)$, at $\nu = 1/n$, it follows that

$$S_{d_1 d_1}(k = 2\pi\nu p) = 4N\nu^2(1-\delta_{k,0}), \quad (16)$$

where $4N\nu^2$ is the maximum possible value for $S_{d_1 d_1}(k)$; it also follows that

$$S_{d_1 d_1}(k \neq 2\pi\nu p) = 0. \quad (17)$$

At special fillings $\nu = \frac{1}{2}, \frac{1}{3}$, and $\frac{1}{4}$, correlation function values, obtained in Eqs. (12) and (13) for CDW state, are in complete agreement with those in Fig. 4(b); furthermore, Fig. 4(c) exactly matches with Eq. (16) at wavevector $k = 2\pi\nu$ and with Eq. (17) when $k \neq 2\pi\nu$. The fact that the structure factor peaks at $k = 2\pi\nu$ at all fillings (including $\nu \neq 1/n$) is in agreement with experimental observations [7, 20]. Furthermore, at $\nu = 1/n$, the peaks at $k = 2\pi\nu$ attain their maximum possible value (indicating charge order) similar to the case in Fig. 4 of Ref. 6 where the peak at $k = 2\pi\nu$ is at its allowed maximum by being approximately equal to the peak at $k = 0$. Next, at $\nu \neq 1/n$, peak values are sizeably smaller than the maximum possible value $4N\nu^2$ much like the situation in Ref. 6 where peak values at $k = 2\pi\nu$ are much smaller than those at $k = 0$. Here, it should be pointed out that our structure factor at $k = 0$ becomes zero and not its maximum [as in Fig. 4 of Ref. 6] because in the definition of $S(k)$ [in Eq.(11)] we subtracted the mean-field term $S^m_{d_1 d_1}(k) = \frac{4}{N}\sum_{j,l} e^{ikl}\langle n_{1,j}\rangle\langle n_{1,j+l}\rangle = 4N\nu^2\delta_{k,0}$.

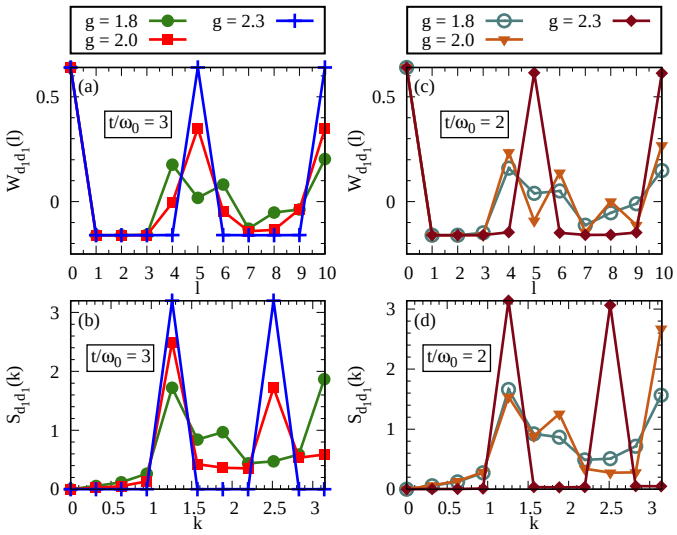

FIG. 5. (Color online) At various values of the electron-phonon coupling g and adiabaticity t/ω_0, comparison of two-point correlation function $W_{d_1 d_1}(l)$ and structure factor $S_{d_1 d_1}(k)$ at filling $\nu = \frac{1}{5}$ and $N = 20$ sites in a straight chain with periodic boundary condition. CDW occurs only at large values of g with modulation wavevector $k = 2\pi\nu$.

At the special filling $\nu = 1/2$, NNN repulsion, NNNN repulsion, and NNNNN repulsion, in the total effective Hamiltonian of Eq. (9) are small compared to the strong NN repulsion term. Therefore, it is the NN and NNN hopping terms in Eq. (9) that compete with the NN repulsion term. For realistic values of adiabaticity and coupling relevant to the manganites, NN repulsion is extremely large compared to either of the hopping terms and this leads to a CDW state at half filling. Similarly, at $\frac{1}{3}$ filling repulsion terms up to NNN and at $\frac{1}{4}$ filling repulsion terms up to NNNN will be relevant and will compete with the NN and NNN hopping terms.

We will now present arguments to show that, in the absence of disorder, the system is metallic away from special fillings $\nu = 1/n$. At fillings $1/3 < \nu < 1/2$, our effective Hamiltonian in Eq. (9) can be represented by a $t_1 - t_2 - V_1 - V_2$ model of spinless fermions where t_1 and t_2 are the NN and NNN hopping terms, respectively; V_1 and V_2 are the NN and NNN repulsion terms with $V_1 >> V_2 >> t_2 \gtrsim t_1$. By using arguments employed in Refs. 40 and 43, this $t_1 - t_2 - V_1 - V_2$ model can be further simplified. Due to the large NN repulsion V_1, with each particle we associate a vacant site adjacent to it (say, on the right side of the particle). Then by deleting all the vacant sites that are adjacent on the right-side of the particles and having only a NN repulsion $V = V_2$ in the reduced system of $N - N_p$ sites, we get the same eigenenergy spectrum. The effective model for Eq. (9) is

$\nu=\frac{1}{2}$		$\nu=\frac{1}{3}$		$\nu=\frac{1}{4}$		$\nu=\frac{1}{5}$		$\nu\neq 1/n$ gap		
N	$\Delta_{\rm gap}$	N	$\Delta_{\rm gap}$	N	$\Delta_{\rm gap}$	N	$\Delta_{\rm gap}$	N	N_p	E_1-E_0
8	1.05882359	12	0.47879386	8	0.00687992	10	0.00008676	10	1	0.00000157
10	1.05882359	18	0.47879391	12	0.00688947	20	0.00009598	20	1	0.00000157
12	1.05882359			16	0.00689015			20	2	0.00000205
14	1.05882359			20	0.00689020			20	3	0.00000159
16	1.05882359									

TABLE I. Excitation gap $\Delta_{\rm gap}$ at special fillings $\nu=1/2$, 1/3, 1/4, and 1/5 and lowest excitation energy (E_1-E_0) at $\nu\neq 1/n$ when electron-phonon coupling $g=2.3$, adiabaticity $\frac{t}{\omega_0}=3.0$, and the system has N_p particles in N sites. Here, energies are in units of $\frac{t^2}{2E_p+2V_p}$. $\Delta_{\rm gap} >> (E_1-E_0)$ indicates CDW.

the following reduced t_1-t_2-V model

$$t_1\sum_k (d^\dagger_{1,k+1}d_{1,k}+\text{H.c.})$$
$$+t_2\sum_k P_{k+1}\left[d^\dagger_{1,k+2}d_{1,k}+\text{H.c.}\right]+V\sum_k n_{1,k}n_{1,k+1},$$

at fillings $1/2<\nu=N_p/(N-N_p)<1$ and with a new nearest-neighbor repulsion $V=V_2$. Next, at fillings $1/4<\nu<1/3$, Eq. (9) can be represented by a $t_1-t_2-V_1-V_2-V_3$ model with V_3 being the NNNN repulsion and $V_2>>V_3>>t_2\gtrsim t_1$; this model can again be reduced to the above t_1-t_2-V model at fillings $1/2<\nu=N_p/(N-2N_p)<1$ and with a new nearest-neighbor repulsion $V=V_3$. Similarly, the case of fillings $1/5<\nu<1/4$ can be represented by a $t_1-t_2-V_1-V_2-V_3-V_4$ model where V_4 is the NNNNN repulsion with $V_3>>V_4>>t_2\gtrsim t_1$; here too the effective model is the reduced t_1-t_2-V model at filling $1/2<\nu=N_p/(N-3N_p)<1$ and with a new nearest-neighbor repulsion $V=V_4$. We observe that the reduced effective t_1-t_2-V model at $1/2<\nu<1$ is effectively a t_1-V model as NNN hopping is not possible at $1/2<\nu<1$; thus our system is a Luttinger liquid and hence is metallic. However, in the presence of even weak disorder, the effective Hamiltonian in Eq. (9) yields an insulating behavior due to one-dimensionality. Here it should be pointed out that a source of disorder in manganites is alkaline-earth doping. Lastly, to calculate the correlation functions, we note that one needs to use the effective Hamiltonian in Eq. (9) and not the reduced t_1-t_2-V model.

We will now discuss the effect of adiabaticity and electron-phonon coupling on CDW. When the electron-phonon coupling g and adiabaticity t/ω_0 are varied in the physically reasonable ranges $1.8\leq g\leq 2.3$ and $2.0\leq t/\omega_0\leq 3.0$, the system remains in a CDW state at the special fillings $\frac{1}{2}$, $\frac{1}{3}$, and $\frac{1}{4}$. On the other hand, at $\nu=1/5$ and in the adiabaticity region $2.0\leq t/\omega_0\leq 3.0$, the system develops a CDW only at large values of g (i.e., $g\approx 2.3$) as shown in Fig. 5 and Table. I. Lastly, at fillings $\nu<1/5$, the system will be metallic; however, introducing disorder will make the one-dimensional system insulating.

1. *Types of chains and ordering at special fillings $\nu=1/n$*

In this section, at special fillings $\nu=1/n$, we will compare the various possibilities depicted in Fig. 6 for the charge/orbital ordered ferromagnetic chains that are antiferromagnetically coupled [44]. In Figs. 6(a), 6(c),and 6(f), the dominant interaction is $-\frac{t^2}{2E_p+2V_p+\alpha_v V_p}$ where $0<\alpha_v<2$; in fact, it can be shown that $\alpha_v=25/32$. On the other hand, in Figs. 6(d) and 6(g), the dominant term is $-\frac{t^2}{2E_p+2V_p}$. Hence, clearly the chain in Fig. 6(d) [Fig. 6(g)] is energetically favorable compared to the chain in Fig. 6(c) [Fig. 6 (f)]. Thus we see that the Wigner-crystal arrangement associated with Fig. 6(d) [Fig. 6(g)] should be preferred over the bi-stripe arrangement associated with Fig. 6(c) [Fig. 6(f)] at filling $\nu=1/3$ [$\nu=1/4$].

In Fig. 6(b), the dominant interaction is $-\frac{t^2}{2E_p+2V_p+2V_p}$; hence, the bent chain in Fig. 6(a) has lower energy compared to the straight chain in Fig. 6(b). Next, in Fig. 6(d) [Fig. 6(g)], the NNNN [NNNNN] interaction obtained due to the left-side electron virtually hopping (to the right and returning) in a fourth-order [sixth-order] perturbation theory in the case of the bent chain is given by $-\frac{t^4}{(2E_p+2V_p)^2(2E_p+\alpha_v V_p)}\left[-\frac{t^6}{(2E_p+2V_p)^2(2E_p)^2(2E_p+\alpha_v V_p)}\right]$; whereas, for the straight chain in Fig. 6(e) [Fig. 6(h)], the corresponding NNNN [NNNNN] interaction is given by $-\frac{t^4}{(2E_p+2V_p)^2(2E_p+2V_p)}\left[-\frac{t^6}{(2E_p+2V_p)^2(2E_p)^2(2E_p+2V_p)}\right]$. Thus, we see that the Wigner-crystal order pertaining to Fig. 6(d) [Fig. 6(g)] is energetically preferred over the C-AFM state in Fig. 6(e)

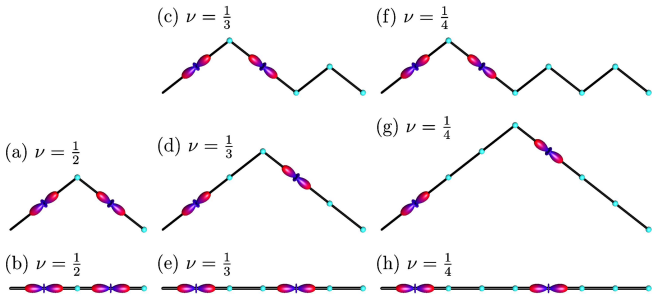

FIG. 6. (Color online) Building blocks with charge/orbital order possibilities for intermediate- and narrow-band manganites. Chain in (a) refers to CE-type order. Straight chains in (b), (e), and (h) represent C-chains. Zigzag chains in (c) and (f) correspond to bi-stripe order whereas bent chains in (d) and (g) represent Wigner-crystal order. In (a), (c), (f) dominant interaction is $-\frac{t^2}{2E_p+2V_p+\alpha_v V_p}$ with $0<\alpha_v<2$; whereas, in (d) and (g) dominant term is $-\frac{t^2}{2E_p+2V_p}$. Clearly, (d) is preferred over (c) while (g) is preferred over (f). In (b) dominant interaction is $-\frac{t^2}{2E_p+2V_p+2V_p}$ implying bent chain in (a) is preferred over straight chain in (b); similar reasoning explains why (d) [(g)] is preferred over (e) [(h)].

[Fig. 6(h)].

Lastly, at $\nu = 1/5$, if the NNN hopping term is more important than the interaction from sixth-order perturbation $-\frac{t^6}{(2E_p+2V_p)^2(2E_p)^3}$, the energy (essentially from the kinetic part) is lower for the straight chain than for the bent chain because the NNN hopping over the bend is smaller (by a factor of half) compared to the NNN hopping along the straight chain. Consequently, at $\nu = 1/5$, the straight chain (without CDW order) is preferred over the bent chain; additionally, straight chain without CDW will continue to be preferred even for $\nu < 1/5$ and we get C-AFM order (instead of a Wigner crystal) at $\nu \leq 1/5$ as witnessed in LCMO [23].

B. Above half-filing case

For the situation where the CJT system is above half-filling, we display the lowest energies as a function of number of d_2-electrons in Fig. 7(a). In the ground state, we observe that the electrons occupy both d_{z^2} and $d_{x^2-y^2}$ orbitals and that the system has degenerate states identifiable by the number (N_2) of d_2-electrons in the degenerate state. For $1/2 < \nu < 1$, the number of degenerate states in a ground state is given by $N_p - \frac{N}{2}$. Now, to understand the site occupancy in the ground state, we note that there is no repulsion between a pair of either d_1-electron and d_2-electron or two d_2-electrons [as can be seen in Eq. (9)]. For the above half-filling case, in order to avoid the large NN repulsion between d_1-electrons, $\frac{N}{2}$ electrons occupy d_{z^2} orbitals in a sub-lattice and excess electrons occupy $d_{x^2-y^2}$ orbitals at random sites in the remaining sub-lattice. Degenerate states with different values of N_2 arise from the fact that a d_1-electron sandwiched between two d_2-electrons can be replaced by a d_2-electron without altering the energy when the onsite inter-orbital repulsion is infinite. This degeneracy keeps the charge ordering intact, though, it destroys the orbital ordering. In the realistic situation of large but finite onsite inter-orbital repulsion, the configuration with the lowest number of d_2-electrons yields the lowest energy as it permits virtual hopping of the d_1-electron to a site with a d_2-electron and returning back.

Next, at $\nu > 1/2$ when both d_1-electrons and d_2-electrons are present, we study correlation functions and structure factors. If all the d_1-electrons belong to one sub-lattice and the d_2 electrons belong to the other sub-lattice, then for all odd values of $l = l_{\rm odd}$ we obtain $\langle n_{a,j} n_{a,j+l}\rangle = 0$ and for all even values of $l = l_{\rm even}$ we get $\langle n_{a,j} n_{b,j+l}\rangle = 0$ with $a \neq b$. Consequently, Eq. (10) yields

$$W_{d_a d_a}(l_{\rm odd}) = -\frac{4N_a^2}{N^2}, \tag{18}$$

where $a = 1, 2$ and

$$W_{d_a d_b}(l_{\rm even}) = -\frac{4N_a N_b}{N^2}, \tag{19}$$

with $a \neq b$. If the d_2-electrons occur randomly in one sub-lattice, for $l = l_{\rm odd}$ and $a \neq b$, we get the simplification $\langle n_{a,j} n_{b,j+l}\rangle = 2\langle n_{a,j}\rangle\langle n_{b,j+l}\rangle$; then, Eq. (10) reduces to

$$W_{d_a d_b}(l_{\rm odd}) = \frac{4N_a N_b}{N^2}. \tag{20}$$

Furthermore, at wavevector $k = \pi$, the structure factor expressed in Eq. (11) simplifies to its maximum possible

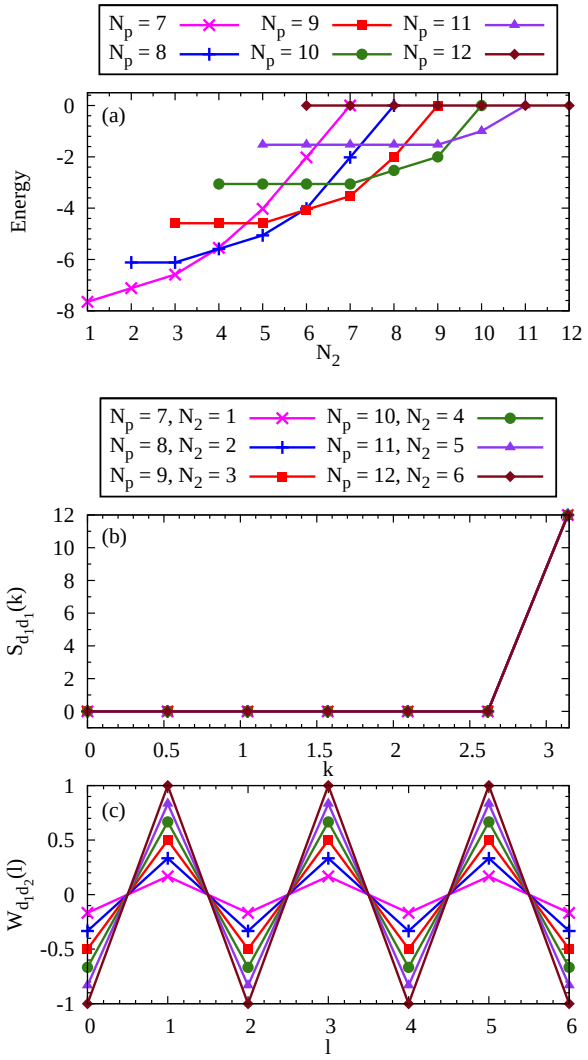

FIG. 7. (Color online) Display of (a) lowest energy (in units of $\frac{t^2}{2E_p+2V_p}$) excluding the polaronic energy; (b) structure factor $S_{d_1 d_1}(k)$; and (c) correlation function $W_{d_1 d_2}(l)$ at filling factor $\nu > 1/2$ in a straight chain with periodic boundary condition. The chain has $N = 12$ sites and N_p electrons of which N_2 are d_2-electrons; the d_2-electrons occupy Jahn-Teller compatible sites just as d_{z^2} electrons in CE-phase of PCMO [19]. The coupling $g = 2.3$ and adiabaticity $\frac{t}{\omega_0} = 3.0$. The structure factor is non-zero only at the reported wavevector $k = \pi$ [7, 20] with a value $S_{d_1 d_1}(k = \pi) = 4N_1^2/N$; the correlation function takes the fixed values $W_{d_1 d_2}(l_{\rm odd}) = -W_{d_1 d_2}(l_{\rm even}) = 4N_1 N_2/N^2$.

value [40]:

$$[S_{d_a d_a}(k=\pi)] = \frac{4N_a^2}{N}. \quad (21)$$

We display the structure factor for d_1-electrons in Fig. 7(b). The structure factor peaks at the wavevector $k = \pi$ and zero everywhere else indicating a CDW at the reported ordering wavevector $k = \pi$ [7, 20]; the peak value $[S_{d_1 d_1}(k = \pi) = 12$ is in agreement with the value given by Eq. (21). Hence, above half filling, all the d_1-electrons reside only in one sub-lattice to avoid large NN repulsion between them. Finally, we depict the correlation between d_1-electrons and d_2-electrons in Fig. 7(c). The function $W_{d_1 d_2}(l)$ oscillates with peaks at odd values of l agreeing with Eq. (20) and lowest points at even values of l concurring with Eq. (19). Hence, above half filling, while d_1-electrons occupy one sub-lattice, d_2-electrons reside randomly in the other sub-lattice. Furthermore, since a NN pair of d_1-electron and d_2-electron do not interact [as shown in Eq. (9)], we note that the d_2-electrons occupy Jahn-Teller compatible sites just as d_{z^2} electrons in CE-phase of PCMO at $0.3 < x < 0.5$ [19].

Therefore, above half filling, system always remains in a CDW state and an orbital-density-wave state both with the same ordering wavevector $k = \pi$.

IV. CONCLUSION

Transition-metal oxides offer considerable scientific and technological opportunities [49]. An effective Hamiltonian (such as ours) for the CJT effect is a needed building block for modeling oxides and for aiding material synthesis.

Duality transformation is a valuable tool in understanding strongly interacting systems in condensed matter physics, statistical physics, quantum field theory, and string theory [45–48]. In this work, we demonstrate that the polaronic (Lang-Firsov) transformation is actually a duality transformation which maps a strong-coupling, many-body problem (where the perturbation is proportional to $g\omega_0/t$) to a weak-coupling, tractable many-body problem (where the small parameter is proportional to $t/(g\omega_0)$). Using perturbation theory (up to sixth order), we obtain our effective Hamiltonian containing the dominant terms for interactions at various distances.

Employing our effective Hamiltonian, we find that cooperative Jahn-Teller interaction in two-band manganites $R_{1-x}A_xMnO_3$ breaks the particle-hole symmetry, i.e., ordering wavevector $k = 2\pi(1-x)$ [$k = \pi$] for doping fraction $x \geq 0.5$ [$x < 0.5$]. Our cooperative picture favors a Wigner-crystal order over bi-stripe order at special fillings 1/3 and 1/4, thereby shedding light on an existing controversy. Additionally, at $\nu = 1/2$, 1/3, and 1/4, we show that zigzag chains (pertaining to Wigner-crystal order) are energetically favorable compared to straight chains; on the other hand, at a lower filling $\nu = 1/5$, we demonstrate that straight chains pertaining to C-AFM order can be realized. Lastly, even within a strong-coupling picture, we show for fillings $\nu \neq 1/n$ that electron diffraction patterns can have finite-peak intensities at wavevector $k = 2\pi\nu$.

In future, we would like to apply our approach to other transition-metal oxides such as nickelates, cobaltates, etc. and study charge stripes at various fillings.

V. ACKNOWLEDGMENTS

One of us (S.Y.) acknowledges the hospitality of the TCM group in the Cavendish Laboratory (Univ. of Cambridge) during the initial part of this work. We thank P. Littlewood, N. D. Mathur, D. E. Khmelnitskii, K. Pradhan, and A. Ghosh for useful discussions.

Appendix A: General Hamiltonian and Derivation of CJT Model

The general Hamiltonian for the CJT system in manganites can be written as $H^G = H_t + H_{ep} + H_l$, where H_t is the hopping term, H_{ep} the electron-phonon-interaction term, and H_l the lattice term. We start with an overcomplete basis $\psi_x = 3x^2 - r^2, \psi_y = 3y^2 - r^2, \psi_z = 3z^2 - r^2$ which satisfies the relation $\psi_x + \psi_y + \psi_z = 0$. The basis state ψ_z corresponds to the d_{z^2} orbital depicted in Fig.1. The hopping term can be expressed in the above basis as:

$$H_t = -t \sum_{i,j,k} [\{d^\dagger_{x^2;i+1,j,k} d_{x^2;i,j,k} + d^\dagger_{y^2;i,j+1,k} d_{y^2;i,j,k} + d^\dagger_{z^2;i,j,k+1} d_{z^2;i,j,k}\} + \text{H.c.}], \quad (A1)$$

where $d^\dagger_{x^2;i,j,k}, d^\dagger_{y^2;i,j,k}, d^\dagger_{z^2;i,j,k}$ are creation operators at the site (i, j, k) for d_{x^2}, d_{y^2}, and d_{z^2} orbitals, respectively. The labeling indices i, j, and k run along the x-, y-, and z-axes, respectively. The electron-phonon interaction term can be written as:

$$H_{ep} = -g\omega_0\sqrt{2M\omega_0} \sum_{i,j,k} [n_{x^2;i,j,k} Q_{x;i,j,k} + n_{y^2;i,j,k} Q_{y;i,j,k} + n_{z^2;i,j,k} Q_{z;i,j,k}], \quad (A2)$$

where g is the electron-phonon coupling, M is the mass of an oxygen ion, ω_0 is the frequency of optical phonons, and $n_{x^2(y^2,z^2);i,j,k} = d^\dagger_{x^2(y^2,z^2);i,j,k} d_{x^2(y^2,z^2);i,j,k}$ are the number operators. Furthermore, $Q_{x;i,j,k}$, $Q_{y;i,j,k}$ and $Q_{z;i,j,k}$ are defined in terms of the displacements [$u_{x;i,j,k}$ & $u_{x;i-1,j,k}$; $u_{y;i,j,k}$ & $u_{y;i,j-1,k}$; $u_{z;i,j,k}$ & $u_{z;i,j,k-1}$] of oxygen ions around (and in the direction of) the d_{x^2}, d_{y^2}, and d_{z^2} orbitals, respectively, as follows: $Q_{x;i,j,k} = u_{x;i,j,k} - u_{x;i-1,j,k}$, $Q_{y;i,j,k} = u_{y;i,j,k} - u_{y;i,j-1,k}$, and $Q_{z;i,j,k} = u_{z;i,j,k} - u_{z;i,j,k-1}$. Here, besides considering the displacement of the ions, we also consider their kinetic energy, thereby invoking quantum

nature of the phonons. Then, the lattice Hamiltonian is given by

$$H_l = \frac{M}{2}\sum_{i,j,k}[\dot{u}^2_{x;i,j,k} + \dot{u}^2_{y;i,j,k} + \dot{u}^2_{z;i,j,k}] + \frac{K}{2}\sum_{i,j,k}[u^2_{x;i,j,k} + u^2_{y;i,j,k} + u^2_{z;i,j,k}], \quad \text{(A3)}$$

where $\dot{u}_{x;i,j,k}$, $\dot{u}_{y;i,j,k}$, and $\dot{u}_{z;i,j,k}$ are the time derivatives of the oxygen-ion displacements $u_{x;i,j,k}$, $u_{y;i,j,k}$, and $u_{z;i,j,k}$, respectively.

The usual orthogonal basis states $\psi_{x^2-y^2}$ and ψ_{z^2} are related to the over-complete basis states ψ_x, ψ_y, and ψ_z as follows:

$$\psi_{x^2-y^2} = \frac{1}{\sqrt{3}}(\psi_x - \psi_y),$$
$$\psi_{z^2} = \psi_z. \quad \text{(A4)}$$

From Eq. (A4) we get,

$$\psi_x = \frac{1}{2}(\sqrt{3}\psi_{x^2-y^2} - \psi_{z^2}),$$
$$\psi_y = -\frac{1}{2}(\sqrt{3}\psi_{x^2-y^2} + \psi_{z^2}),$$
$$\psi_z = \psi_{z^2}. \quad \text{(A5)}$$

Next, using Eq. (A5), we express the general Hamiltonian in the orthogonal basis $\psi_{x^2-y^2}$ and ψ_{z^2} as follows:

$$H_t = -\frac{t}{4}\sum_{i,j,k}\{(d^\dagger_{z^2;i+1,j,k}, d^\dagger_{x^2-y^2;i+1,j,k})\begin{pmatrix}1 & -\sqrt{3}\\ -\sqrt{3} & 3\end{pmatrix}\begin{pmatrix}d_{z^2;i,j,k}\\ d_{x^2-y^2;i,j,k}\end{pmatrix} + \text{H.c.}\} - \frac{t}{4}\sum_{i,j,k}\{(d^\dagger_{z^2;i,j+1,k}, d^\dagger_{x^2-y^2;i,j+1,k}) \times \begin{pmatrix}1 & \sqrt{3}\\ \sqrt{3} & 3\end{pmatrix}\begin{pmatrix}d_{z^2;i,j,k}\\ d_{x^2-y^2;i,j,k}\end{pmatrix} + \text{H.c.}\} - t\sum_{i,j,k}\{(d^\dagger_{z^2;i,j,k+1}, d^\dagger_{x^2-y^2;i,j,k+1})\begin{pmatrix}1 & 0\\ 0 & 0\end{pmatrix}\begin{pmatrix}d_{z^2;i,j,k}\\ d_{x^2-y^2;i,j,k}\end{pmatrix} + \text{H.c.}\}, \quad \text{(A6)}$$

$$H_{ep} = -\frac{1}{4}g\omega_0\sqrt{2M\omega_0} \times \sum_{i,j,k}(d^\dagger_{z^2;i,j,k}, d^\dagger_{x^2-y^2;i,j,k})\begin{pmatrix}Q_{x;i,j,k} + Q_{y;i,j,k} + 4Q_{z;i,j,k} & -\sqrt{3}Q_{x;i,j,k} + \sqrt{3}Q_{y;i,j,k}\\ -\sqrt{3}Q_{x;i,j,k} + \sqrt{3}Q_{y;i,j,k} & 3Q_{x;i,j,k} + 3Q_{y;i,j,k}\end{pmatrix}\begin{pmatrix}d_{z^2;i,j,k}\\ d_{x^2-y^2;i,j,k}\end{pmatrix}, \quad \text{(A7)}$$

and H_l is again given by Eq. (A3). Here, it should be mentioned that an expression for H^G in an alternate basis has been derived in Ref. 50; however, these authors consider classical phonons.

Now, we consider a one-dimensional Jahn-Teller chain with cooperative electron-phonon interaction along the z-direction and non-cooperative electron-phonon interaction (of the Holstein-type [36, 37]) along the x- and y-directions as shown in Fig. 1 of the main text. The lattice term given by Eq. (A3) can be written for this case as follows:

$$H_l^{CJT} = \frac{M}{2}\sum_k[\dot{u}^2_{x;0,k} + \dot{u}^2_{x;1,k} + \dot{u}^2_{y;0,k} + \dot{u}^2_{y;1,k} + \dot{u}^2_{z;k}] + \frac{K}{2}\sum_k[u^2_{x;0,k} + u^2_{x;1,k} + u^2_{y;0,k} + u^2_{y;1,k} + u^2_{z;k}]. \quad \text{(A8)}$$

We define $Q'_{x;k} \equiv u_{x;1,k} + u_{x;0,k}$, $Q'_{y;k} \equiv u_{y;1,k} + u_{y;0,k}$, $Q_{x;k} \equiv u_{x;1,k} - u_{x;0,k}$, and $Q_{y;k} \equiv u_{y;1,k} - u_{y;0,k}$ and incorporate these definitions in Eq. (A8) to obtain

$$H_l^{CJT} = \frac{M}{2}\sum_k\left[\frac{1}{2}\{\dot{Q}'^2_{x;k} + \dot{Q}'^2_{y;k}\} + \frac{1}{4}\{\dot{Q}^{+2}_{xy;k} + \dot{Q}^{-2}_{xy;k}\} + \dot{u}^2_{z;k}\right] + \frac{K}{2}\sum_k\left[\frac{1}{2}\{Q'^2_{x;k} + Q'^2_{y;k}\} + \frac{1}{4}\{Q^{+2}_{xy;k} + Q^{-2}_{xy;k}\} + u^2_{z;k}\right], \quad \text{(A9)}$$

where $Q^{\pm}_{xy;k} \equiv Q_{x;k} \pm Q_{y;k}$. For the present single-chain case, Eqs. (A6) and (A7) reduce to the following equations:

$$H_t^{CJT} = -t\sum_k(d^\dagger_{z^2;k+1}d_{z^2;k} + \text{H.c.}), \quad \text{(A10)}$$

and

$$\frac{H_{ep}^{CJT}}{g\omega_0\sqrt{2M\omega_0}} = -\sum_k \Big[\Big\{(u_{z;k}-u_{z;k-1})+\frac{1}{4}Q^+_{xy;k}\Big\}d^\dagger_{z^2;k}d_{z^2;k} + \frac{3}{4}Q^+_{xy;k}d^\dagger_{x^2-y^2;k}d_{x^2-y^2;k} - \frac{\sqrt{3}}{4}Q^-_{xy;k}\Big(d^\dagger_{z^2;k}d_{x^2-y^2;k}+\text{H.c.}\Big)\Big]. \quad \text{(A11)}$$

Next, we note that the center-of-mass displacement terms $Q'_{x;k}$ and $Q'_{y;k}$ as well as the center-of-mass momentum terms $\dot{Q}'_{x;k}$ and $\dot{Q}'_{y;k}$ of Eq. (A9) do not couple to the electrons [as can be seen from Eqs. (A10) and (A11)]. Hence, for our single-chain case, Eq. (A9) simplifies to be

$$H_l^{CJT} = \sum_k\left[\frac{1}{2}M\dot{u}^2_{z;k}+\frac{1}{2}Ku^2_{z;k}\right] + \sum_k\left[\frac{1}{2}\frac{M}{4}\dot{Q}^{+2}_{xy;k}+\frac{1}{2}\frac{K}{4}Q^{+2}_{xy;k}\right] + \sum_k\left[\frac{1}{2}\frac{M}{4}\dot{Q}^{-2}_{xy;k}+\frac{1}{2}\frac{K}{4}Q^{-2}_{xy;k}\right]. \quad \text{(A12)}$$

The general Hamiltonian for the present CJT single chain can be expressed as follows by adding Eqs. (A10), (A11), and (A12):

$$H^{CJT} = H_t^{CJT}+H_{ep}^{CJT}+H_l^{CJT}. \quad \text{(A13)}$$

Next, by using the following second-quantized representation of the various displacement operators:

$$u_{z;k}=\frac{a^\dagger_{z;k}+a_{z;k}}{\sqrt{2M\omega_0}}, Q^+_{xy;k}=\frac{b^\dagger_k+b_k}{\sqrt{2\frac{M}{4}\omega_0}}, Q^-_{xy;k}=\frac{c^\dagger_k+c_k}{\sqrt{2\frac{M}{4}\omega_0}},$$

in the above Hamiltonian of Eq. (A13), we obtain

$$H^{CJT} = -t\sum_k(d^\dagger_{z^2;k+1}d_{z^2;k}+\text{H.c.}) - g\omega_0\sum_k\Big[(a^\dagger_{z;k}+a_{z;k})(n_{z^2;k}-n_{z^2;k+1}) + \frac{1}{2}(b^\dagger_k+b_k)(n_{z^2;k}+3n_{x^2-y^2;k}) - \frac{\sqrt{3}}{2}(c^\dagger_k+c_k)(d^\dagger_{z^2;k}d_{x^2-y^2;k}+\text{H.c.})\Big] + \omega_0\sum_k(a^\dagger_{z;k}a_{z;k}+b^\dagger_kb_k+c^\dagger_kc_k), \quad \text{(A14)}$$

where $n_{z^2;k} \equiv d^\dagger_{z^2;k}d_{z^2;k}$ and $n_{x^2-y^2;k} \equiv d^\dagger_{x^2-y^2;k}d_{x^2-y^2;k}$.

Appendix B: Perturbation up to second-order

We adopt a polaronic transformation for the Hamiltonian in Eq. (1) of the main text so that we can perform perturbation theory. In the polaronic frame of reference, the transformed Hamiltonian reads $\tilde{H}^{CJT} = \exp(S)H^{CJT}\exp(-S)$ where the operator S is defined in Eq. (2) of the main text. Then, the transformed Hamiltonian can be expressed as $\tilde{H}^{CJT} = H_0 + H_1$ with

$$H_0 = \omega_0\sum_k(a^\dagger_ka_k+b^\dagger_kb_k+c^\dagger_kc_k) - \frac{9}{4}g^2\omega_0\sum_k(n_{1,k}+n_{2,k}) - \frac{3}{2}g^2\omega_0\sum_k n_{1,k}n_{2,k} + 2g^2\omega_0\sum_k n_{1,k}n_{1,k+1} - te^{-\frac{13}{4}g^2}\sum_k(d^\dagger_{1,k+1}d_{1,k}+\text{H.c.}), \quad \text{(B1)}$$

where the term $2g^2\omega_0\sum_k n_{1,k}n_{1,k+1}$ arises because of the cooperative nature of the interaction; furthermore, the attractive interaction term $-\frac{3}{2}g^2\omega_0\sum_k n_{1,k}n_{2,k}$ will be negated by a much larger repulsive Coulombic term $U\sum_k n_{1,k}n_{2,k}$ because of which no site can have both the orbitals occupied simultaneously. Here it is important to point out that there is no interaction between a NN pair of either d_1-electron and d_2-electron or two d_2-electrons. The remaining term of $\tilde{H}^{CJT}$ can be written as $H_1 \equiv H_1^I + H_1^{II}$ with

$$H_1^I = -te^{-\frac{13}{4}g^2}\sum_k[d^\dagger_{1,k+1}d_{1,k}\{\mathcal{T}^{k\dagger}_+\mathcal{T}^k_- - 1\}+\text{H.c.}], \quad \text{(B2)}$$

where $\mathcal{T}^k_\pm \equiv \exp[\pm g(2a_k - a_{k-1} - a_{k+1}) \pm \frac{g}{2}(b_k - b_{k+1})]$ and

$$H_1^{II} = \frac{\sqrt{3}}{2}g\omega_0e^{-\frac{3}{2}g^2}\sum_k(c^\dagger_k+c_k)\Big[d^\dagger_{1,k}d_{2,k} \times e^{g(a^\dagger_{k-1}-a^\dagger_k+b^\dagger_k)}e^{-g(a_{k-1}-a_k+b_k)}+\text{H.c.}\Big]. \quad \text{(B3)}$$

Now, to perform perturbation theory, we note that the eigenstates of H_0 are given by $|n,m\rangle = |n\rangle_{el}\otimes|m\rangle_{ph}$ with $|0,0\rangle$ being the ground state. We consider the case when the coefficients of the perturbation terms H_1^I and H_1^{II} in Eqs. (B2) and (B3), respectively, satisfy the conditions $te^{-\frac{13}{4}g^2} << \omega_0$ and $\frac{\sqrt{3}}{2}ge^{-\frac{3}{2}g^2} << 1$ Now, the first order correction is zero and the second-order perturbation term [obtained using Schrieffer-Wolff transformation as mentioned in Eq. (6) of Ref. 40] is expressed as

$$H^{(2)} = \sum_m\frac{\langle 0|_{ph}H_1|m\rangle_{ph}\langle m|_{ph}H_1|0\rangle_{ph}}{E_0^{ph}-E_m^{ph}}. \quad \text{(B4)}$$

In Eq. (B4), the contribution of cross terms involving H_1^I and H_1^{II} is zero because the phonons do not match; hence, we get

$$H^{(2)} = \sum_m\frac{\langle 0|_{ph}H_1^I|m\rangle_{ph}\langle m|_{ph}H_1^I|0\rangle_{ph}}{E_0^{ph}-E_m^{ph}} + \sum_m\frac{\langle 0|_{ph}H_1^{II}|m\rangle_{ph}\langle m|_{ph}H_1^{II}|0\rangle_{ph}}{E_0^{ph}-E_m^{ph}}. \quad \text{(B5)}$$

We will first evaluate the term involving H_1^{II} in the above equation. After some algebra, we get the following expression:

$$\sum_m \frac{\langle 0|_{ph} H_1^{II}|m\rangle_{ph}\langle m|_{ph} H_1^{II}|0\rangle_{ph}}{E_0^{ph}-E_m^{ph}} \approx -\frac{\omega_0}{4}\sum_k \Big[n_{1,k}+n_{2,k}-2n_{1,k}n_{2,k}\Big]. \quad \text{(B6)}$$

We note that the coefficients of the terms $n_{1,k}$, $n_{2,k}$, and $n_{1,k}n_{2,k}$ in the above equation are much smaller than the coefficients of the same terms in Eq. (B1); consequently, we ignore the contribution from Eq. (B6) in the expression for the effective Hamiltonian of the CJT chain.

Next, we evaluate the term involving H_1^I in Eq. (B5) and obtain:

$$\begin{aligned}
&\sum_m \frac{\langle 0|_{ph} H_1^{I}|m\rangle_{ph}\langle m|_{ph} H_1^{I}|0\rangle_{ph}}{E_0^{ph}-E_m^{ph}} \\
&= -\frac{t^2}{\omega_0} e^{-\frac{13}{2}g^2} G_3\left(2,2,\frac{1}{4}\right)\sum_k \Big[d^\dagger_{1,k+2}(1-n_{1,k+1})(1-n_{2,k+1})d_{1,k}+\text{H.c.}\Big] \\
&\quad -\frac{t^2}{\omega_0} e^{-\frac{13}{2}g^2} G_5\left(4,1,1,\frac{1}{4},\frac{1}{4}\right)\sum_k \Big[n_{1,k}(1-n_{1,k-1})(1-n_{2,k-1})(1-n_{1,k-2})+n_{1,k}(1-n_{1,k+1})(1-n_{2,k+1})(1-n_{1,k+2})\Big] \\
&\quad -(.)\sum_k \Big[n_{1,k}(1-n_{1,k-1})(1-n_{2,k-1})n_{1,k-2}+n_{1,k}(1-n_{1,k+1})(1-n_{2,k+1})n_{1,k+2}\Big], \qquad \text{(B7)}
\end{aligned}$$

where the coefficient [denoted by (.)] of the last term on the RHS will be given below and $G_n(\alpha_1,\alpha_2,\ldots,\alpha_n)\approx \frac{e^{\sum_{i=1}^n \alpha_i g^2}}{\sum_{i=1}^n \alpha_i g^2}$ for large values of g^2 (see Appendix C for details).

Then, on using the above approximation for $G_n(\alpha_1,\alpha_2,\ldots,\alpha_n)$ at large g^2, Eq. (B7) simplifies as follows:

$$\begin{aligned}
&\sum_m \frac{\langle 0|_{ph} H_1^{I}|m\rangle_{ph}\langle m|_{ph} H_1^{I}|0\rangle_{ph}}{E_0^{ph}-E_m^{ph}} \\
&= -\frac{4}{17}\frac{t^2}{g^2\omega_0} e^{-\frac{9}{4}g^2}\sum_k \Big[d^\dagger_{1,k+2}(1-n_{1,k+1})(1-n_{2,k+1})d_{1,k}+\text{H.c.}\Big] \\
&\quad -\frac{2}{13}\frac{t^2}{g^2\omega_0}\sum_k \Big[n_{1,k}(1-n_{1,k-1})(1-n_{2,k-1})(1-n_{1,k-2})+n_{1,k}(1-n_{1,k+1})(1-n_{2,k+1})(1-n_{1,k+2})\Big] \\
&\quad -\left(\frac{t^2}{2E_p+4V_p}\right)\sum_k \Big[n_{1,k}(1-n_{1,k-1})(1-n_{2,k-1})n_{1,k-2}+n_{1,k}(1-n_{1,k+1})(1-n_{2,k+1})n_{1,k+2}\Big], \qquad \text{(B8)}
\end{aligned}$$

where the coefficients of the first and second terms on the RHS agree with the corresponding terms in Eq. 6 in the main text; then, the coefficient of the last term on the RHS is identified from Eq. 6 in the main text.

Appendix C: Simplification of the function $G_n(\alpha_1,\alpha_2,\ldots,\alpha_n)$

In this appendix, we obtain simple expressions for the function $G_n(\alpha_1,\alpha_2,\ldots,\alpha_n)$ appearing in Appendix B. The general term $G_n(\alpha_1,\alpha_2,\ldots,\alpha_n)$ is defined as

$$G_n(\alpha_1,\alpha_2,\ldots,\alpha_n) \equiv F_n(\alpha_1,\alpha_2,\ldots,\alpha_n) + \sum_{k=1}^{n-1}\sum_c F_k(\alpha_{c_1},\alpha_{c_2},\ldots,\alpha_{c_k}),$$

where

$$F_n(\alpha_1,\ldots,\alpha_n) \equiv \sum_{m_1=1}^{\infty}\ldots\sum_{m_n=1}^{\infty}\frac{(\alpha_1 g^2)^{m_1}\ldots(\alpha_n g^2)^{m_n}}{m_1!\ldots m_n!(m_1+\ldots+m_n)},$$

and the summation over c represents summing over all possible ${}^nC_k$ combinations of k arguments chosen from the total set of n arguments $\{\alpha_1,\alpha_2,\ldots,\alpha_n\}$.

We evaluate the derivative of the general term $G_n(\alpha_1,\alpha_2,\ldots,\alpha_n)$ with respect to g^2:

$$\begin{aligned}
&g^2\frac{d}{dg^2}G_n(\alpha_1,\alpha_2,\ldots,\alpha_n) \\
&= (e^{\alpha_1 g^2}-1)(e^{\alpha_2 g^2}-1)\ldots(e^{\alpha_n g^2}-1) \\
&\quad +\sum_{k=1}^{n-1}\sum_c (e^{\alpha_{c_1} g^2}-1)(e^{\alpha_{c_2} g^2}-1)\ldots(e^{\alpha_{c_k} g^2}-1) \\
&= \Big[\Pi_{i=1}^n\big\{(e^{\alpha_i g^2}-1)+1\big\}\Big]-1 \\
&= e^{\sum_{i=1}^n \alpha_i g^2}-1. \qquad \text{(C1)}
\end{aligned}$$

Then, the general term is obtained to be

$$G_n(\alpha_1, \alpha_2, \ldots, \alpha_n) = \int \frac{e^{\sum_{i=1}^{n} \alpha_i g^2} - 1}{g^2} dg^2 = \int \sum_{m=1}^{\infty} \frac{(\sum_{i=1}^{n} \alpha_i)^m (g^2)^{(m-1)}}{m!} dg^2 = \sum_{m=1}^{\infty} \frac{(\sum_{i=1}^{n} \alpha_i g^2)^m}{m\, m!}. \quad \text{(C2)}$$

For large values of g^2, we have the approximation

$$\int \frac{e^{\sum_{i=1}^{n} \alpha_i g^2} - 1}{g^2} dg^2 \approx \frac{e^{\sum_{i=1}^{n} \alpha_i g^2}}{\sum_{i=1}^{n} \alpha_i g^2}.$$

Appendix D: Depiction of fourth-order processes

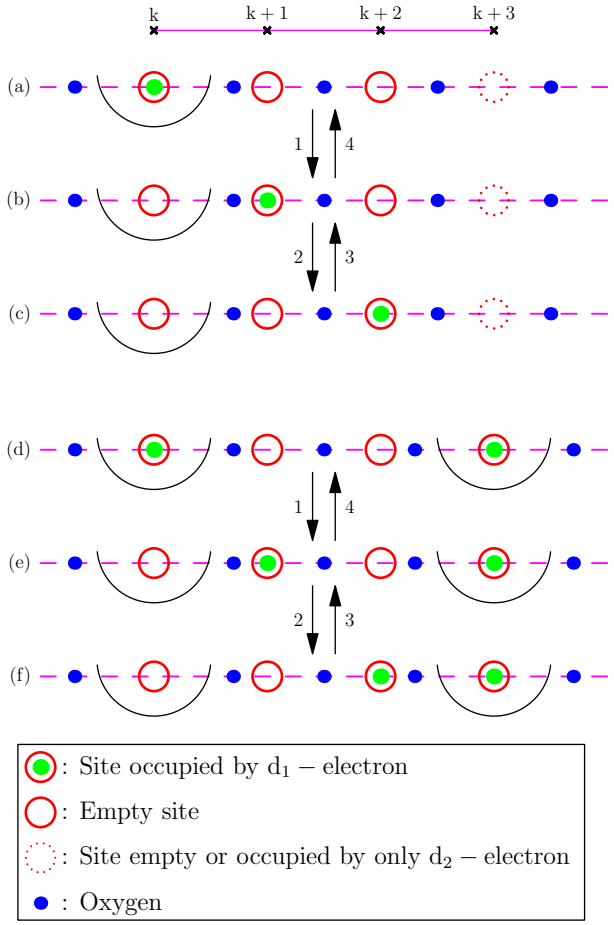

FIG. 8. (Color online) Display of initial/final and intermediate states with concomitant lattice distortions in a fourth-order perturbation process involving electron hopping right to NNN site and returning. When NNNN site is unoccupied by d_1-electron, we depict initial/final state (a); intermediate states (b) and (c). When NNNN site is occupied by d_1-electron, we show initial/final state (d); intermediate states (e) and (f). The numbered arrows indicate the order of hopping.

[1] M. v. Zimmermann, C. S. Nelson, J. P. Hill, Doon Gibbs, M. Blume, D. Casa, B. Keimer, Y. Murakami, C.-C. Kao, C. Venkataraman, T. Gog, Y. Tomioka, and Y. Tokura, Phys. Rev. B **64**, 195133 (2001).

[2] S. Larochelle, A. Mehta, N. Kaneko, P. K. Mang, A. F. Panchula, L. Zhou, J. Arthur, and M. Grevena, Phys. Rev. Lett. **87**, 095502 (2001).

[3] Z. Jirák, S. Krupička, Z. Šimša, M. Dlouhá, S. Vratislav, J. Magn. Magn. Mater. **53**, 153 (1985).

[4] C. H. Chen, S.-W. Cheong, and H. Y. Hwang, J. Appl. Phys. **81**, 4326 (1997).

[5] C. H. Chen, S. Mori, and S.-W. Cheong, Phys. Rev. Lett. **83**, 4792 (1999).

[6] J. C. Loudon, S. Cox, A. J. Williams, J. P. Attfield, P. B. Littlewood, P. A. Midgley, and N. D. Mathur, Phys. Rev. Lett. **94**, 097202 (2005).

[7] G. C. Milward, M. J. Calderón, and P. B. Littlewood, Nature **433**, 607 (2005).
[8] P. G. Radaelli et al., Phys. Rev. B **55**, 3015 (1997).
[9] P. G. Radaelli et al., Phys. Rev. B **59**, 14440 (1999).
[10] R. Wang, J. Gui, Y. Zhu, and A. R. Moodenbaugh, Phys. Rev. B **61**, 11946 (2000).
[11] J. García *et al.*, J. Phys. Condens. Matter **13**, 3243 (2001).
[12] J. Rodríguez-Carvajal et al., Physica B (Amsterdam) **320**, 1 (2002).
[13] M. T. Fernández-Díaz *et al.*, Phys. Rev. B **59**, 1277 (1999).
[14] M. Hervieu et al., Eur. Phys. J. B **8**, 31 (1999).
[15] J. M. Tranquada *et al.*, Nature (London) **375**, 561 (1995).
[16] C. H. Chen, S.-W. Cheong, and A. S. Cooper, Phys. Rev. Lett. **71**, 2461 (1993).
[17] M. Cwik *et al.*, Phys. Rev. Lett. **102**, 057201 (2009).
[18] V. J. Emery, S. A. Kivelson, and J. M. Tranquada, Proc. Natl. Acad. Sci. USA **96**, 8814 (1999).
[19] Y. Tokura, Rep. Prog. Phys. **69**, 797 (2006).
[20] H. Ulbrich and M. Braden, Physica C **481**, 31 (2012).
[21] M. B. Salamon and M. Jaime, Rev. Mod. Phys. **73**, 583 (2001).
[22] Z. Jirák, S. Krupička, and Z. Šimša, J. Magn. Magn. Mater. **53**, 153 (1985).
[23] M. Pissas and G. Kallias, Phys. Rev. B **68**, 134414 (2003).
[24] M. Pissas, I. Margiolaki, K. Prassides, and E. Suard Phys. Rev. B **72**, 064426 (2005).
[25] S. Mori, C. H. Chen, and S.-W. Cheong, Nature **392**, 473 (1998).
[26] P. N. Santhosh, J. Goldberger, P. M. Woodward, T. Vogt, W. P. Lee, and A. J. Epstein, Phys. Rev. B **62**, 14928 (2000).
[27] A. Lanzara, N. L. Saini, M. Brunelli, F. Natali, A. Bianconi, P. G. Radaelli, and S.-W. Cheong, Phys. Rev. Lett. **81**, 878 (1998).
[28] D. Louca, T. Egami, E. L. Brosha, H. Röder, and A. R. Bishop, Phys. Rev. B **56**, R8475 (1997).
[29] J. Goodenough, Phys. Rev. **100**, 564 (1955).
[30] A. J. Millis, P. B. Littlewood, and B. I. Shraiman, Phys. Rev. Lett. **74**, 5144 (1995).
[31] T. V. Ramakrishnan, H. R. Krishnamurthy, S. R. Hassan, and G. Venketeswara Pai, Phys. Rev. Lett. **92**, 157203 (2004).
[32] R. K. Zheng, R. X. Huang, A. N. Tang, G. Li, X. G. Li, J. N. Wei, J. P. Shui, and Z. Yao, Appl. Phys. Lett. **81**, 3834 (2002).
[33] R. K. Zheng, G. Li, A. N. Tang, Y. Yang, W. Wang, X. G. Li, Z. D. Wang, and H. C. Ku, Appl. Phys. Lett. **83**, 5250 (2003).
[34] P. Tong, Bongju Kim, Daeyoung Kwon, Bog G. Kim, G. Y. Ahn, J. M. S. Park, Sung Baek Kim, and S-W. Cheong Appl. Phys. Lett. **93**, 202504 (2008).
[35] T. F. Seman, K. H. Ahn, T. Lookman, A. Saxena, A. R. Bishop, and P. B. Littlewood, Phys. Rev. B **86**, 184106 (2012).
[36] T. Holstein, Ann. Phys. (N.Y.) **8**, 343 (1959).
[37] S. Datta, A. Das, and S. Yarlagadda, Phys. Rev. B **71**, 235118 (2005).
[38] I. G. Lang and Y. A. Firsov, Zh. Eksp. Teor. Fiz. **43**, 1843 (1962) [Sov. Phys. JETP **16**, 1301 (1963)].
[39] S. Reja, S. Yarlagadda, and P. B. Littlewood, Phys. Rev B **84**, 085127 (2011).
[40] R. Pankaj and S. Yarlagadda, Phys. Rev. B **86**, 035453 (2012).
[41] For a perturbative analysis of the Holstein model in the original laboratory frame of reference when $g\omega_0/t$ is small, see S. Datta and S. Yarlagadda Phys. Rev. B **75**, 035124 (2007).
[42] E. R. Gagliano, E. Dagotto, A. Moreo, and F. C. Alcaraz, Phys. Rev. B **34**, 1677 (1986).
[43] S. Reja, S. Yarlagadda, and P. B. Littlewood, Phys. Rev. B **86**, 045110 (2012).
[44] For a classification of bi-stripe structure and Wigner-crystal structure based on winding number, see T. Hotta, Y. Takada, H. Koizumi, and E. Dagotto Phys. Rev. Lett. **84**, 2477 (2000).
[45] S. Sachdev, Ann. Rev. Condens. Matter Phys. **3**, 9 (2012).
[46] J. B. Kogut, Rev. Mod. Phys. **51**, 659 (1979).
[47] R. Savit, Rev. Mod. Phys. 52, 453 (1980).
[48] J. Polchinski, Rev. Mod. Phys. **68**, 1245 (1996).
[49] J. Chakhalian, A. J. Millis, and J. Rondinelli, Nat. Mater. **11**, 92 (2012).
[50] P. B. Allen and V. Perebeinos, Phys. Rev. B **60**, 10747 (1999).